Energy Storage Materials 45 (2022) 484–493

Contents lists available at ScienceDirect

Energy Storage Materials

journal homepage: www.elsevier.com/locate/ensm

Synergistic effects of chlorine substitution in sulfide electrolyte solid state batteries

Eva Gil-González[a,1], Luhan Ye[a,1], Yichao Wang[a,1], Zulipiya Shadike[b], Zhenming Xu[a], Enyuan Hu[b], Xin Li[a,*]

[a] John A. Paulson School of Engineering and Applied Sciences, Harvard University, Cambridge, MA 02138, USA
[b] Chemistry Division, Brookhaven National Laboratory, Upton, NY 11973, USA

A B S T R A C T

All-solid-state battery is considered as one of the most promising competitors to Li ion batteries. Two widely known performance metrics for solid electrolytes, among others, are ionic conductivity and stability. Here it is found that both can be improved by the synergistic effects of chlorine substitution in sulfide-based solid electrolytes. Particularly, instabilities arising from both bulk decompositions and interfacial reactions to electrodes can be better inhibited in the chlorine substituted sulfide solid electrolytes through the increased susceptibility to the mechanical constriction induced enhancement of voltage stability. As a result, the stability window of some chlorine-rich Li-argyrodites can be systematically higher than some other chlorine-deficient or chlorine-free electrolytes, especially under the implementation of the mechanical constriction battery assembly and test conditions. Thus, a solid-state battery system of 4 V to 5 V-class cathodes paired with lithium metal anode is demonstrated using these chlorine-rich Li-argyrodites without additional coatings. Furthermore, since Cl composition modulates the stability and instability of Li-argyrodite at low voltages, it allows us to design a multilayer configuration with a hierarchy of Li metal stabilities to demonstrate the stable cycling at relatively high current densities for solid-state batteries. It is found that a moderate Cl composition in the electrolyte is the best to inhibit Li dendrite penetration as the central electrolyte layer, emphasizing a slightly increased "instability" as the hidden performance metric of relevance here, in addition to the two well-known metrics of stability and ionic conductivity. The understanding of the chlorine substitution effect in sulfide electrolytes provides an important design principle for all-solid-state batteries.

1. Introduction

All-solid-state battery is one of the most promising next generation mobile energy storage technologies, due to its potential for high energy and power densities as well as the mitigation of safety issues of traditional lithium-ion batteries [1–4]. This is mostly attributed to the advances in the development of solid electrolytes [5–7]. Sulfide-based solid electrolytes have attracted great attention with reported conductivity values of up to 25 mS cm^{-1} for $Li_{9.54}Si_{1.74}P_{1.44}S_{11.7}Cl_{0.3}$ (LSPSCl) [8], which are comparable and even higher than those of traditional liquid electrolytes [9]. Li-argyrodites fall within this type of sulfide solid electrolyte, with the general formula $Li_{7-y}PS_{6-y}X_y$ (traditionally: $y \leq 2$ and X = halogen atom) [10] and ionic conductivities beyond 1 mS cm^{-1}. [11–13]

The main role of the partial substitution of sulfur by a halogen atom is to stabilize the high temperature phase in which the pure Li-argyrodite, Li_7PS_6, crystallizes, as its macroscopic value of ionic conductivity is several orders of magnitude higher than that of the low temperature phase [14,15]. This substitution has been traditionally restricted to one halogen per formula. Nevertheless, a computational work performed by Klerk et al. predicted that the increase of chlorine content can lead to an optimum occupancy of Cl over the 4a and 4c sites (1:3 ratio) that increases, although not significantly, Li-ion conductivity in theoretical compositions such as $Li_5PS_4Cl_2$. [16] From an experimental point of view, it has been confirmed that higher amount of halogen substitution can indeed increase the conductivity in the chlorine-rich argyrodites family of $Li_{6-y}PS_{5-y}Cl_{1+y}$ ($y < 1$), with $Li_{5.5}PS_{4.5}Cl_{1.5}$ (LPSCl1.5) being the end member of the series [17–20], even though $Li_5PS_4Cl_2$ was predicted to be thermodynamically stable [16]. Nevertheless, this chlorine-rich Li-argyrodite, LPSCl1.5, exhibits ionic conductivity values as high as 10 mS cm^{-1} in cold pressed specimens [18,19].

Besides high ionic conductivity, wide stability window is another important requirement for solid electrolyte. For LPSCl1.5 and Li_6PS_5Cl (LPSCl1.0), it has been reported that their experimental voltage windows are quite narrow, ranging from 1.8 to 2.5 V[19] and from 1.3 to 2.3 V[21], respectively. The 1.3 ~ 2.3 V of LPSCl1.0 is wider than the computational prediction of 1.7 - 2.0 V based on thermodynamic convex hull approach [22]. Considering that sulfide electrolytes in the cathode region are often mixed with conductive carbon in these experimental electrochemical tests [19,21,23,24], this in principle allows the electron transfer together with certain Li^+ capacity from the electrolyte. A computational investigation first explored this effect that can possibly expand the volt-

* Corresponding author.
E-mail address: lixin@seas.harvard.edu (X. Li).
[1] Equal Contribution

https://doi.org/10.1016/j.ensm.2021.12.008
Received 27 September 2021; Received in revised form 22 November 2021; Accepted 7 December 2021
Available online 9 December 2021

age window of $Li_xGeP_2S_{12}$ to 1.0 - 3.0 V[25] from the thermodynamic 1.7 - 2.1 V of $Li_{10}GeP_2S_{12}$[22] (LGPS). Experimentally, LGPS was later made as both cathode and anode in a single battery [24], demonstrating that the Li capacity does exist in sulfide electrolytes. More recently, it was shown that by taking into account the Li^+ capacity effect, the calculated voltage window can be expanded to 1.1 - 2.2 V[21] for LPSCl1.0, which is closer to the 1.3 - 2.3 V measured experimentally in the same work, compared with the 1.7 - 2.0 V in simulation without considering this effect.

It is worth noting, however, although in the above experiments the ceramic samples were cold pressed with high pressure, the metal anode layer was only gently attached to the electrolyte layer without an adequate press, as lithium or lithium alloy may be squeezed through the electrolyte layer under high external pressure. Similarly, the electrochemical tests were under no or weak operational stack pressure (a few MPa or below) during the battery test. On the contrary, the voltage windows of LGPS were reported to be up to 5 V[26] and 10 V[27] under a high operational stack pressure (30 to 400 MPa), which is consistent with the stable battery cycling performance using 4 - 5 V cathodes tested under similar conditions [8,26,28]. This suggests that at least the operational voltage window of sulfide electrolytes tested under a sufficient stack pressure is much wider than the predictions based on either the thermodynamic convex hull approach [22] or with the Li^+ capacity effect considered [21,25].

We showed that without a sufficient stack pressure there is at least 10 to 20% porosity left in the ceramic pellet after the cold press, while with a stack pressure larger than 25 MPa, the porosity could be minimized to nearly zero [27]. We believe the zero-porosity condition in the ceramic layers is critical to the implementation of the mechanical constriction condition, as the constriction will be lifted at any voids. Our previous works show that particles with a close contact can mechanically constrict each other locally, providing an effective modulus on the order of the material's mechanical modulus at the GPa level to modulate electrochemical reactions. The mechanical constriction effect can significantly widen the voltage window of sulfide electrolytes through metastability up to around 3.5 to 4 V[27,29–32], because in order for a reaction with positive reaction strains to happen, it will have to overcome the extra metastable barrier induced by mechanically constricted local environment. The effect can further widen the voltage window through kinetic stability up to 10 V[27,31], because the positive reaction strains, if generated by decompositions that have overcome the metastable barrier, may cause a local compressive strain field surrounding the decomposition front to suppress the local ionic interdiffusion by orders of magnitude. This ionic passivation will self-limit the propagation of local decompositions. The effect also modifies the decomposition reaction pathway to form less reduced valence states in the anode [30] and less oxidized ones in the cathode [27] for certain elements in the electrolyte, as reaction pathways will be modulated by both metastability and kinetic stability induced by the constriction.

Note that the wide operational voltage window [26,27] and good cycling performance [8,26,28] with high voltage cathodes can be demonstrated no matter with the conductive carbon added to the cathode [8] or not [26–28], as long as the mechanical constriction is properly implemented [33], suggesting that ionic passivation dominates over electronic passivation here. Specifically, the conductive carbon mixed in the cathode [8], the electronic conductivity of uncoated cathode particles [27,28], and the very slow scanning speed of 0.1 mV/s in the cyclic voltammetry test [27] suggest that the electronic passivation at least will not dominate the voltage stability region of 4 to 10 V under a constricted condition.

Here in this paper, we show that by the application of mechanical constriction condition, the calculated voltage window of the superionic chlorine-doped Li-argyrodite, including LPSCl1.5, LPSCl1.0, $Li_{6.5}PS_{5.5}Cl_{0.5}$ (LPSCl0.5), can be widened by metastability to as wide as 0.8- 4.3 V predicted by our unique constrained ensemble computational platform [29,33]. Interestingly, it was found previously that further increasing Cl composition to $Li_5PS_4Cl_2$ (LPSCl2.0) makes the argyrodite cubic phase difficult to synthesize, while an orthorhombic phase can be obtained in experiment [34]. We find here in our calculation that the orthorhombic LPSCl2.0 shows an even wider voltage window of 0.1 - 4.7 V and a significantly reduced decomposition energy at 0 V with Li metal. This is due to the higher reaction strains of the chlorine-related decomposition products than that of other sulfide electrolytes without or with lower chlorine content in their compositions, such as from $Li_7P_3S_{11}$ (LPS), LGPS and LSPSCl. The higher reaction strain contributes to a larger response of chlorine-doped electrolytes in the voltage window expansion to the mechanical constriction effect. Meanwhile, the degree of electronic passivation is shown to be much less changed by chemical compositions, based on our circuit model by considering all the decomposition phases in the calculation. However, our calculated Li ion conductivity peaks at LPSCl1.5, i.e., the end member of the argyrodite phase with Cl doping, and drops at the orthorhombic phase of LPSCl2.0.

Furthermore, previously we demonstrated that superionic chlorine-rich Li-argyrodite of LPSCl1.5 can show good cycling performances even in a direct contact with lithium metal anode and high voltage cathodes [28]. The wide voltage window for LPSCl1.5 down to around 0 V and beyond 4.3, i.e., beyond the predicted metastable voltage window of 0.8 - 4.3 V in our calculation, indicates the general importance of kinetic stability due to ionic passivations [27,28]. This is also why in our recent work that combines LPSCl1.5 with LGPS into a multilayer configuration, LPSCl1.5 is considered as a more stable electrolyte with Li metal, while LGPS is the less stable one [28]. Here in this work a further comparison of LPSCl1.5 with LPSCl1.0, LPSCl0.5, LPS and LGPS electrolytes with different Cl compositions shows that LPSCl1.5 can be considered as functionally stable with Li metal, while others cannot, likely suggesting the additional importance of the compositional proximity of cubic LPSCl1.5 to orthorhombic LPSCl2.0, as the orthorhombic LPSCl2.0 shows an outstanding voltage window in the series of $LPSCl_x$ (x = 0, 0.5, 1.0, 1.5, 2.0) with our constrained ensemble prediction.

Since the multilayer configuration utilizes a combination of more stable and less stable electrolyte layers to Li metal for the Li dendrite suppression, we thus combine the more stable LPSCl1.5 with the other two $LPSCl_x$ (x = 1.0 and 0.5) electrolytes, all within the argyrodite cubic phase, into various multilayer configurations, to demonstrate a superior cycling performance of solid-state batteries at high current densities up to 5 to 10 mA/cm^2. Furthermore, we show that similar cathode-electrolyte interface decompositions can give different cycling performances, which instead emphasizes the importance of the anode interphase to the cycling performance of solid-state batteries when LPSCl1.5 is used as the cathode electrolyte.

The understanding here provides new insights into the chemical design and optimization of solid electrolytes for all-solid-state batteries. The synergistic effect of chlorine substitution in Li-argyrodite leads to a concomitant process that not only increases the ionic conductivity but also widens the electrochemical voltage window. The results also unveil how different interface reaction strains and decomposition energies, as well as their multilayer combinations control the solid-state battery performance.

2. Results and discussion

2.1. The synergistic effects of Cl substitution

As mentioned, two important criteria for solid electrolytes are high ionic conductivity and wide stability window. Fig. 1a shows the calculated stability window and ionic conductivity values of different sulfide-based solid electrolytes (SEs) as a function of Cl content in their compositions. The stability window has been calculated based on the Gibbs free energy differential form of $G'(x_D)$:

$$\partial_{x_D} G' = G_D - G_{SE} + \partial_{x_D} G_{strain} \quad (1)$$

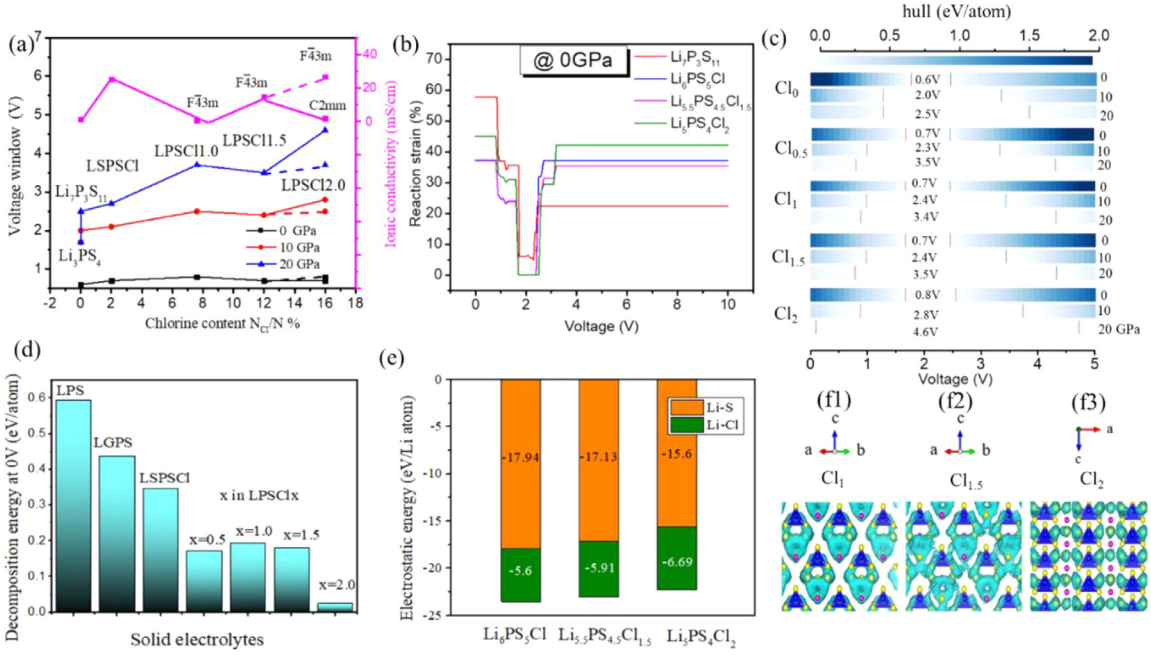

Fig. 1. (a) Voltage window and ionic conductivity as a function of chlorine content for different sulfide-based solid electrolytes, including $Li_7P_3S_{11}$, Li_3PS_4, $Li_{20}Si_3P_3S_{23}Cl$ (LSPSCl), Li_6PS_5Cl (LPSCl1.0), $Li_{5.5}PS_{4.5}Cl_{1.5}$ (LPSCl1.5), $Li_5PS_4Cl_2$ (LPSCl2.0). Space groups for $Li_{7-x}PS_{6-x}Cl_x$ have also been labeled. LPSCl1.0 and LPSCl1.5 are the cubic F-43 m phase, while for LPSCl2.0, the C2mm phase is represented by solid lines and the F-43 m one is represented by dashed lines. (b) reaction strain (at K_{eff} = 0 GPa) versus voltage window for sulfide-based SEs with different chlorine contents in the composition. (c) Exact stability window at different mechanical constrictions (K_{eff} = 0, 10 and 20 GPa) for $Li_7P_3S_{11}$ (Cl_0) and $Li_{7-x}PS_{6-x}Cl_x$ (x = 0.5, 1.0, 1.5, and 2.0). The color represents the level of reaction energy, where darker color corresponds to higher reaction energy. (d) Decomposition energies of $Li_7P_3S_{11}$ (LPS), LGPS, LSPSCl, $Li_{7-x}PS_{6-x}Cl_x$ (x = 0.5, 1.0, 1.5, and 2.0) at 0 V at 20 GPa. (e) Electrostatic energy of $Li_{7-x}PS_{6-x}Cl_x$ (x = 1.0, 1.5, and 2.0). (f) Lithium ion probability density distribution (light blue) in $Li_{7-x}PS_{6-x}Cl_x$, x = 1.0 (f1), 1.5 (f2) and 2.0 (f3), from 900 K AIMD simulations with an isosurface value of 0.0015 a_0^{-3} (a_0 is the Bohr radius). Note that for LPSCl2.0, except for (a), where both cubic and orthorhombic phases are presented, all other panels only consider the synthesizable orthorhombic phase.

which is determined by the chemical term ($\delta G^0 = G_D - G_{SE}$) and the strain term ($\partial_{x_D} G_{strain} = V \epsilon_{RXN} K_{eff}$), where ϵ_{RXN} and K_{eff} are the reaction strain and the effective bulk modules, respectively. The stability window is decided by the intrinsic decomposition energy change, which is related to the composition and structure of solid electrolytes. In practice, we want to emphasize that solid electrolytes are usually constrained in a rigid local environment during battery testing, thus this mechanical constriction effect leads to a metastable state ($\partial_{x_D} G'(x_D = 0) > 0$). The reaction strain and the exact stable window for $Li_7P_3S_{11}$ (LPS) and $LPSCl_x$ family at different K_{eff} are shown in Figures 1b and 1c, respectively.

In Fig. 1 (and Supplementary Figure S1) it is observed that under mechanical constriction, the voltage stability windows can be classified into three categories, the narrow type of no-Cl or low-Cl compositions (LPS, LGPS, LSPSCl) of up to around 2.0 at%; the medium type of $LPSCl_x$ (x = 0.5, 1.0, 1.5) with Cl content from 3.7 to 12 at%, which covers all the synthesizable Li-argyrodites; and the wide type of LPSCl2.0 with a Cl content of 16.7 at%. The widened stability window is attributed to both the intrinsic stability of cubic argyrodite and the orthorhombic structures under mechanical constriction, and the higher reaction strain caused by Cl doping at low and high voltages at no constriction (Fig. 1b), where the Cl-free $Li_7P_3S_{11}$ is compared with other Cl-rich compositions.

More detailed comparisons between $Li_7P_3S_{11}$ and Cl doped $LPSCl_x$ (x = 1.0, 1.5, 2.0), together with another common electrolyte LGPS, can be found in the Supporting Information (SI), including their decomposition energies and strains (Figure S1), and the exact reaction equations of decomposition products (Table S1 - S3), within each voltage range at different K_{eff} . In Table S1 - S3, we also calculated the pseudo-bandgap and pseudo-resistivity for the decomposition interphase based on our circuit model (Figure S2) using the data of band gaps and molar volume of each decomposition product (Table S4). As included in Table S4, in the high voltage range, the decomposition products of the Cl-rich solid electrolyte, LPSCl1.5, consist of Cl-related compounds (PCl_3, SCl, SCl_4) that generally have higher molar volume than those decomposition products of Cl-free electrolytes, such as phosphorous sulfides, i.e. Li_2PS_3 and P_2S_7. Consequently, the reaction strain in the high voltage range is higher in the Cl-rich solid electrolytes, as demonstrated in Figures 1b and S1.

This voltage stabilization effect is more notable at high mechanical constrictions, represented by the effective bulk modules (K_{eff}) (Fig. 1a and 1c, Figure S1). It should be noted that sulfide electrolyte solid state batteries usually work with an external pressure applied, which is on the order of MPa. Such an external pressure, however, can generate a mechanically constrictive environment due to the reduction of porosity of the ceramic pellet to nearly 0% [27]. The effective modules (K_{eff}) are therefore on the order of the mechanical modulus of solid electrolytes, that is at GPa level, experienced by any local electrolyte decompositions with a positive reaction strain. This concept is discussed in depth in our previous works [27,29-32]. Depending on the mechanical constriction condition, systems can range from isobaric (K_{eff} = 0) to isovolumetric (K_{eff} = infinite) conditions, where the expected values of K_{eff} in real battery systems are on the order of 10 - 20 GPa based on the bulk modulus of sulfide ceramics (20–40 GPa) and cathode materials (>100 GPa), and the battery assembly and test procedures [29,33].

For instance, the stability window for $LPSCl_x$ (x = 0.5, 1.0, 1.5) is widened from around 1.8 - 2.4 V at K_{eff} = 0 GPa to 0.8 - 4.3 V at K_{eff} = 20 GPa (Fig. 1c). Importantly, for K_{eff} in the range from 20 GPa to 0 GPa, the reaction energy of LPSCl1.5 at 0 V varies from 0.25 to 1.5 eV/atom, which is much smaller than that of $Li_7P_3S_{11}$ and LGPS in the range from 0.5 to 2–2.5 eV/atom. This results in a much more stable interphase with Li metal for LPSCl1.5, which is generally true for $LPSCl_x$ at x = 0.5 - 1.5, as shown in Fig. 1d and S1. It is worth noting that the voltage window of LPSCl2.0 is the widest (0.1 - 4.7 V at K_{eff} = 20 GPa), and the decomposition energy of 0.024 eV/atom at 0 V is also the low-

est among $LPSCl_x$. This is mainly due to the experimental orthorhombic phase, as the corresponding values for the cubic argyrodite LPSCl2.0 are 0.7 - 4.4 V and 0.145 eV/atom at 0 V at K_{eff} = 20 GPa. This also suggests that as the end member of argyrodite $LPSCl_x$, the LPSCl1.5 phase is likely to show a wider experimental voltage window and enhanced voltage stability due to the proximity to the orthorhombic LPSCl2.0, as any Cl composition fluctuation in LPSCl1.5 is likely to generate the more stable LPSCl2.0 nano-phase locally.

On the other hand, based on our circuit model (Figure S2) that considers the volume ratio and related percolation of each decomposition phase, the overall interphase formed by decomposition products show a similar global electronic resistivity for $LSPCl_x$, $Li_7P_3S_{11}$ and LGPS in the entire voltage range, and they are largely insulating electronically at low voltages and become more conductive at high voltages (Tables S1- S3). The careful computational examination here suggests that electronic passivation is much less susceptible to chemical compositions than the mechanical constriction effect in governing the different voltage stabilities of sulfide electrolytes. That is, a lower stability at 0 V is most probably not caused by the lack of electronic insulation, but rather a weaker effect of mechanical constriction induced voltage stability; while a higher stability at cathode voltages is most probably not caused by an electronically less conductive decomposition interphase, but rather a stronger effect of mechanical constriction induced voltage stability. Such constriction induced stabilities at both cathode and anode voltage ranges could include the effects of metastability and kinetic stability, as described previously [27,30].

We further study the effect of Cl substitution on the ionic conductivity. A series of long-time simulations based on ab initio molecular dynamics (AIMD) at elevated temperatures were performed for the Li-argyrodite family, $Li_{7-x}PS_{6-x}Cl_x$ (x = 1.0, 1.5), and the orthorhombic phase at x = 2.0. The AIMD calculated activation energies E_a for $Li_{7-x}PS_{6-x}Cl_x$ (x = 1.0, 1.5 and 2.0) are 325.48, 230.24 and 292.62 meV, respectively, and the corresponding room-temperature conductivities are estimated to be 0.43, 14.55 and 1.69 mS cm^{-1} (Figure S3). The ionic conductivities first increase and then decrease with Cl substitution, showing a maximum at x = 1.5. Note that the space group for $1 \leq x \leq 1.5$ is F-43 m, whereas for x = 2 it is C2mm. These data, along with the calculated conductivity values of other solid electrolytes in Fig. 1a, are in a good agreement with those reported in the literature by either experiment or computation listed in Table S5. However, it is noteworthy that certain dispersion of experimental data for a given electrolyte can be attributed to different experimental synthesis and test conditions.

To further understand the atomistic diffusion mechanisms and pathways of the Li-argyrodite family, we calculated the electrostatic energy of each lithium atom and the Li ion probability density distribution and direction projected mean square displacement (MSD) of Li ion from 900 K AIMD simulations, as shown in Figures 1e, 1f and S4. The normalized electrostatic energy is calculated by counting the interaction of lithium with all surrounding anions and then dividing by the amount of lithium. Monovalent halogen anions interact more weakly with lithium cations than divalent sulfur anions, which leads to the decrease of the normalized electrostatic energy with Cl substitution [35]. Theoretically, the activation energy of the electrolyte should be linearly decreased correspondingly. However, it can be seen from the lithium ion probability density distributions that structurally there are only cage-like local lithium-ion diffusions in Li_6PS_5Cl (LPSCl1.0) (Fig. 1f1), while in $Li_{5.5}PS_{4.5}Cl_{1.5}$ (LPSCl1.5) there are abundant inter-cage jumps (Fig. 1f2), responsible for the significantly enhanced macroscopic lithium ion diffusion. The main reason may be that the higher amount of monovalent chlorine anions occupies the 4*c* sites in LPSCl1.5, which are fully occupied by divalent sulfur anions in LPSCl1.0, leading to weaker interactions with lithium ions and consequently weakening the cage-like local lithium-ion diffusions.

Nevertheless, when the amount of Cl substitution is higher, such as in $Li_5PS_4Cl_2$ (LPSCl2.0), based on the DFT simulations by S. P Ong et al. [36], the ground state crystal structure is changed to the space group C2mm that is also lower in energy than LPSCl1.0 and LPSCl1.5, as indicated in Fig. 1a. This implies that lithium ion diffusion in LPSCl2.0 along the *c* direction is much faster than those in the *a-b* plane, exhibiting one-dimensional lithium diffusion, as evidenced from lithium ion probability density distribution (Figures 1f3 and S4). In summary, different electrostatic energies and diffusion pathways induce the ionic conductivity changes in the range $1 \leq x \leq 1.5$, while for $x > 1.5$ a phase transition from $F\bar{4}3m$ to C2mm is expected to happen, promoting one-dimensional diffusional pathway and, therefore, decreasing the ionic conductivity. Note that if $F\bar{4}3m$ is adopted for LPSCl2.0, the calculated ionic conductivity can reach up to 26.6 mS cm^{-1}, as also shown in Fig. 1a.

In light of these results, LPSCl1.5 is of a particular interest here, suggested by our computations, because it not only presents the highest value of ionic conductivity, but more importantly, may also possess the highest voltage window within the Li-argyrodite phase, due to the proximity to the orthorhombic LPSCl2.0. This suggests that a layer of LPSCl1.5 may form a more stable primary interface to the Li metal layer. However, as we will show in the next section, $LPSCl_x$ (x = 1.0 and 0.5) are also of interest, and LPSCl1.0 can show a more stable cycling when served as the central or inner layer in a more complicated battery configuration that is not in a direct contact with the Li metal layer. This is likely due to the enhanced “instability” of LPSCl1.0 that balances well with the stability, as an additional counterintuitive metric of a particular relevance here in suppressing the Li dendrite penetration.

2.2. Stability and instability of $LPSCl_x$ at low voltages using lithium metal as anode

The stability and instability of $Li_{5.5}PS_{4.5}Cl_{1.5}$ (LPSCl1.5), Li_6PS_5Cl (LPSCl1.0), $Li_{6.5}PS_{5.5}Cl_{0.5}$ (LPSCl0.5), and $Li_7P_3S_{11}$ (LPS) are further investigated using DFT simulations, electrochemical methods and analytical characterizations. More details about sample preparation and basic characterization can be found in SI (Methods and Figures S5-S6). According to the simulation results presented in the above section, strong mechanical constriction would stabilize more efficiently Cl-rich solid electrolytes (SEs) due to higher reaction strains. Therefore, asymmetric batteries with a configuration of Li/SE/Stainless Steel (SS) were assembled and discharged to deposit Li metal on the surface of SEs, both with and without stack pressures. The deposition surface thus corresponds to approximately a local mechanical constriction K_{eff} values of approaching 20 and 0 GPa, respectively, with and without a stack pressure. Fig. 2a compares the XRD data of the discharged asymmetric batteries of LPSCl1.5 (Cl-rich SE) with those of $Li_7P_3S_{11}$ (Cl-free SE). When testing with no external pressure applied, the XRD pattern of $Li_7P_3S_{11}$ suffers a dramatic change with respect to its pristine one, indicating that the material undergoes severe decompositions, with the production of the Li_2S phase [37] among other products that could not be identified easily. In contrast, the decomposition of LPSCl1.5 is much more limited, where just a few minor decomposition peaks emerge, mainly attributed to Li_2S and elemental phosphorus [38]. These results are also in good agreement with the XRD data shown in Figures S7 a and b, where the chemical stability of LPSCl1.5 versus $Li_7P_3S_{11}$ with Li metal was studied by mixing the electrolyte with Li metal and annealing them at 100 ºC for 6 h under a protective argon atmosphere [39]. This result agrees with our discussion in the previous section that chlorine-rich solid electrolyte possesses better stability than those with lower Cl ratio in their compositions.

In order to gain more insights about the nature of decomposition products of LPSCl1.5 at the Li deposition surface with and without a stack pressure, XPS measurements after Li deposition were conducted and compared with DFT simulations, as shown in Figures 2b and 2c, respectively. Note that Cl 2p spectra does not experience any change, as it was also observed and discussed elsewhere [38,40,41], thus it is not shown. Both P 2p and S 2p spectra are very similar to those of pristine LPSCl1.5 (Figure S7 c). Particularly, the P 2p spectra in pristine LPSCl1.5 can be described by two doublets at approximately 131.7 and 133 eV,

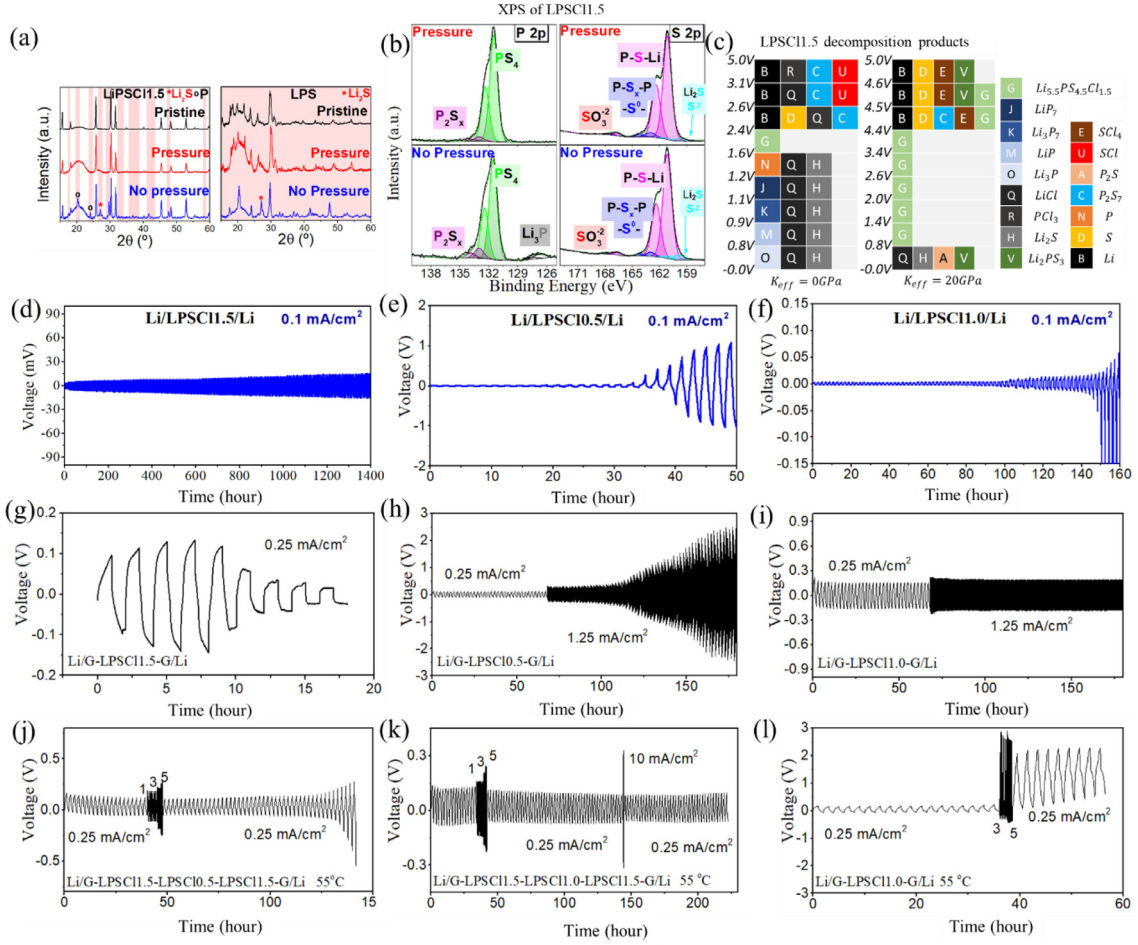

Fig. 2. (a) Ex-situ XRD patterns of LPSCl1.5 and $Li_7P_3S_{11}$ (LPS) after Li deposition in asymmetric batteries (Li/SE/SS)) with and without mechanical constrictions. The operating stack pressure is applied at 100 MPa. SS: stainless steel. (b) P 2p and S 2p XPS spectra in Li/LPSCl1.5/SS cells after Li deposition with and without mechanical constrictions. (c) Decomposition reaction pathways at K_{eff} = 0 and 20 GPa and predicted decomposition products in different phase equilibria within each voltage range. All decomposition products are the ground state phases within each voltage range. (d-f) Stripping/plating behavior in (d) Li/LPSCl1.5/Li cell, (e) Li/LPSCl0.5/Li cell, and (f) Li/LPSCl1.0/Li cell at a current density of 0.1 mA cm^{-2} and continuous 1 h plating/stripping durations. (g-l) Stripping/plating behavior in Li/G-SE-G/Li cell at a current density of 0.25 - 10 mA cm^{-2} with the capacity of 0.25 mAh/cm^2 for each half cycle: SE = (g) LPSCl1.5, (h) LPSCl0.5, (i) LPSCl1.0, (j) LPSCl1.5-LPSCl0.5-LPSCl1.5, (k) LPSCl1.5-LPSCl1.0-LPSCl1.5, and (l) LPSCl1.0, where (j-l) are tested for 10 cycles up to high current densities at 55 °C.

which are associated with PS_4^- tetrahedral units and the presence of polysulfide species (P_2S_x), respectively. The S 2p spectra of pristine LPSCl1.5 is also composed by two doublets, the main one at 161.3 eV accounts for the Li-S-P bonds of Li-argyrodites, whereas the doublet at 163 eV is related to the presence of polysulfide compounds with bridging (-S-) and terminal sulfur bonds (P-S_x-P) [38,40-43]. These polysulfides species may include some remaining P_2S_5 from the synthesis, that cannot be detected by XRD. After the electrochemical deposition of Li in both cells, with or without pressure applied during battery testing, some reductions are observed as shown in Fig. 2b, and as also predicted in Fig. 2c (see also Table S2). Note that the presence of sulfites SO_3^{2-} (167 eV) may be explained by the strong tendency of Li_2S to be oxidized (−1.756 eV/atom) [44], as samples were shortly exposed to air before the transfer to the vacuum chamber of XPS.

The most important result from the combined analysis of XPS and computational prediction is that the mechanical constriction effect may partially inhibit the decomposition and change the decomposition reaction pathway. Particularly, when at no mechanical constriction (K_{eff} = 0 GPa), the low voltage decomposition results in products of lithium binaries (Fig. 2bc, Figure S7c), such as Li_2S, Li_xP_y and LiCl. These products are in good agreement with previous experimental and theoretical predictions [22,38,40]. In contrast, under mechanical constriction ($K_{eff} \approx 20\ GPa$), the production of lithium phosphides-related compounds, Li_xP_y, are suppressed, favoring the decomposition into polysulfide compounds which are likely to be Li_2PS_3 with lower decomposition energy (Figures 2b-c and Tables S1). Furthermore, the application of mechanical constriction also suppresses the decomposition peak of P_2S_x, indicating a further limit of the decomposition.

We further assemble symmetric batteries of Li/SE/Li with the central SE layer being LPSCl1.5, LPSCl1.0 and LPSCl0.5, respectively, and perform cycling tests. We believe this is a more relevant approach to evaluate their functional stabilities for electrochemical performance. Fig. 2d shows a stable long cycling performance of symmetric LPSCl1.5 battery operating at a low current density of 0.1 mA/cm^2, where the overpotential is just 15 mV after 1400 h of operation. In comparison, LPSCl0.5 shows a quick voltage increase after 30 h at the same cycling rate (Fig. 2e), induced by decompositions with Li metal, indicating a worse electrochemical stability against Li metal than LPSCl1.5. LPSCl1.0 is more stable than LPSCl0.5, but it also shows a voltage increase after cycling for about 100 h (Fig. 2f), suggesting that LPSCl1.0 is less stable than LPSCl1.5 in a direct contact with Li metal.

We then apply the Li/Graphite-SE-Graphite/Li structure to avoid the direct contact of Li metal layer with the SE layer in battery assembly and to test higher current densities. The graphite layer in the Li-graphite anode here also acts as a protection to avoid Li penetration induced short circuit when external pressure is applied, while for those unsta-

ble electrolytes with Li metal, the graphite protection layer also plays the role to delay the interface contact from the step of initial battery assembly, where no local mechanical constriction exists, to the step of electrochemical cycling, where Li sufficiently mixes with graphite to eventually contact the electrolyte under a local mechanic constriction condition with suppressed decompositions [45]. LPSCl1.5 quickly shows a short circuit induced sudden drop of polarizations, when the current is increased to 0.25 mA/cm^2 (Fig. 2g), consistent with our recent finding that an elctrochemically more stable electrolyte to Li metal can more easily allow the Li dendrite to penetrate through cracks, as there is no sufficient decompositions to fill the cracks [28]. In contrast, the phenomenon of short circuit does not happen for LPSCl0.5 or LPSCl1.0 at 0.25 mA/cm^2 (Fig. 2h, 2i). Instead, the decomposition induced voltage increase similar to the case without the graphite protection can still be observed from the Li/G-LPSCl0.5-G/Li battery at 1.25 mA/cm^2 (Fig. 2h), confirming that LPSCl0.5 is electrochemically the least stable with Li metal among the three types of LPSCl$_x$.

Interestingly, LPSCl1.0 at the same testing condition (Fig. 2i) shows a longer cycling than LPSCl0.5 and LPSCl1.5, indicating that LPSCl1.0 shows a moderate stability against Li between LPSCl1.5 and LPSCl0.5, or a better balance of stability and instability. That is, LPSCl1.0 is more stable than LPSCl0.5, so it does not show the severe decomposition induced resistance and polarization increase. While it is less stable than LPSCl1.5, so LPSCl1.0 can avoid the Li dendrite penetration induced short circuit through sufficient but self-limiting local decompositions to fill microcracks but without consuming more pristine electrolytes [28]. The finding here is also consistent with the fact that LPSCl1.0 electrolyte can show superior cycling with both Li metal and high voltage cathode [46].

In our recent paper [28], it shows that the multilayer configuration of “more stable”|“less stable”|“more stable” solid electrolytes against Li metal can prevent the dendrite penetration through a self-limiting local decompositions that happened in the inner less-stable electrolyte layer, with the outer more stable layer to provide a better primary interface to Li metal anode layer. Here, the approach is for the first time applied with $Li_{7-x}PS_{6-x}Cl_x$ (x = 0.5, 1.0, and 1.5) of different Cl compositions, so that the stability and instability levels in correlation with the Cl composition in the argyrodite phase can be evaluated in experiment by the unique multilayer approach. LPSCl0.5 as the inner layer and LPSCl1.5 as the outer layer in the multilayer structure (Fig. 2j) can enable the high-rate cycling up to 5 mA/cm^2, performing better at high current densities than any single layer configurations. However, the multilayer battery fails after 130 h cycling, which might be due to the propagation of decompositions in LPSCl0.5.

Furthermore, although LPSCl1.0 shows a similar decomposition energy to LPSCl0.5 (Fig. 1d), it can serve as a relatively better inner layer in the multilayer configuration for a stable cycling of up to 5 to 10 mA/cm^2 (Fig. 2k). However, without multilayer the single layer LPSCl1.0 fails immediately when the current density is higher than 3 mA/cm^2 (Fig. 2l), indicating that it is the utilization of the multilayer rather than solely the chemistry of LPSCl1.0 that enables the high current density capability above 3 mA/cm^2. The failure in Fig. 2l above 3 mA/cm^2 shows a significant increase of polarization after the high current test, suggesting a propagation of decompositions driven by the large current. The solid batteries after 100-hour cycling were disassembled and cross-section SEM images were taken for the batteries with a single solid electrolyte layer and multiple layers (Figure S8). It is found that more cracks occur in the LPSCl1.5 layer while a very limited number of cracks can be observed from the LPSCl1.0 layer. An impedance measurement was conducted before and after cycling (Figure S9). The battery shows a slight increase in the impedance after cycling, which indicates that local decompositions, instead of the short circuit, accumulate during cycling [47].

The comparison between LPSCl0.5, LPSCl1.0 and LPSCl1.5 in Fig. 2, nevertheless, suggests that LPSCl1.0 at the material chemistry level shows a better balance of stability and instability with Li metal when serving as the central or inner layer, so that local decompositions can be used to suppress Li dendrite while without inducing excessive decomposition propagations, for a superior cycling stability (Fig. 2i, 2k). On the contrary, LPSCl1.5 is too stable with Li (Fig. 2d) and can only serve as the outer layer to form a stable primary interface with the Li metal anode layer (Fig. 2d, 2j, 2k). At a slightly higher current density (Fig. 2g), internal short circuit happens quickly with cycling, most probably due to the Li dendrite penetration through cracks in LPSCl1.5 with an insufficient obstruction from local decompositions. LPSCl0.5, on the other hand, seems to be on the side of higher decomposition energy than LPSCl1.0, and hence shows an obvious off-balance toward excessive instability compared with LPSCl1.0, with a worse cycling stability induced by excessive decompositions (Fig. 2e, 2 h, 2j).

Note that LGPS as the central [30] or inner [28] layer can show cycling performance of several thousand hours and up to 10 - 20 mA/cm^2, which is superior to both LPSCl1.0 and LPSCl0.5 as the corresponding layers, while LGPS shows a higher decomposition energy than LPSCl0.5 at 0 V (Fig. 1d). The result here thus suggests a few possibilities: i) LPSCl0.5 and LPSCl1.0 may exhibit a weaker self-limiting ability for the decompositions than LGPS, as described by the thermodynamic metastability metric of critical modulus in our recent work [48], or ii) a weaker kinetic ionic passivation ability at low voltages, as these electrolytes are all largely insulating electronically at low voltages, as we discussed in the previous section regarding the circuit model (Figure S2), or iii) LGPS may show a more complicated structural inhomogeneity to lower the actual decomposition energy, similar to what may have happened in LPSCl1.5. These may result in a better balance of stability and instability in LGPS than LPSCl1.0. However, a more detailed comparison of LGPS with LPSCl$_x$ is beyond the scope of the current paper.

Therefore, the above discussion also suggests that a complicated functionality of solid electrolytes in solid state batteries often cannot be decided by a single parameter, but rather should be evaluated by a balance of multiple metrics. Specifically, higher decomposition energy may not be the only metric for selecting “less stable” electrolytes as the inner layer in the multilayer configuration [28], as demonstrated in the comparison of LPSCl1.0 and LPSCl0.5; while lower decomposition energy should not be misunderstood as the golden metric for the application of Li metal anode, as illustrated by the comparison of LPSCl1.0 and LPSCl1.5. It depends on the position of an electrolyte relative to that of the Li metal anode in a complicated battery configuration, where additional metrics of the decomposition being sufficiently self-limiting through either thermodynamic or kinetic origins, and microstructure controls, could be equally important. The right balance of these metrics may form the opportunity to design a stable Li metal anode battery, the fully understanding of which, however, could be challenging.

2.3. Stability of LPSCl$_x$ with high voltage cathodes

Electrochemical stability of LPSCl1.5 at high voltages was tested by cyclic voltammogram (CV) tests (Figures S10), which shows that under mechanical constriction there is no big decomposition peak in the high voltage region up to 6 V, unlike the liquid electrolyte battery, where no mechanical constriction is applied to the LPSCl1.5 particles. The ex-situ XPS measurements included in Figure S10c well support the CV test results, where, in contrast to the liquid electrolyte battery, there is no evidence of oxidation when sufficient mechanical constriction is applied, suggesting that LPSCl1.5 is also a stable solid electrolyte at high voltages.

It is worth noting that in the high voltage range of Fig. 2c, the presence of Li metal from decomposition reactions in the computational prediction can be localized in the cathode region or electrolyte region toward cathode [31] in experiments by metastability and kinetical stability originated from the mechanical constriction [27]. Although some Li^+ and e^- generated by decompositions with a good conductive pathway in the weakly constrained region can still be transported to the anode

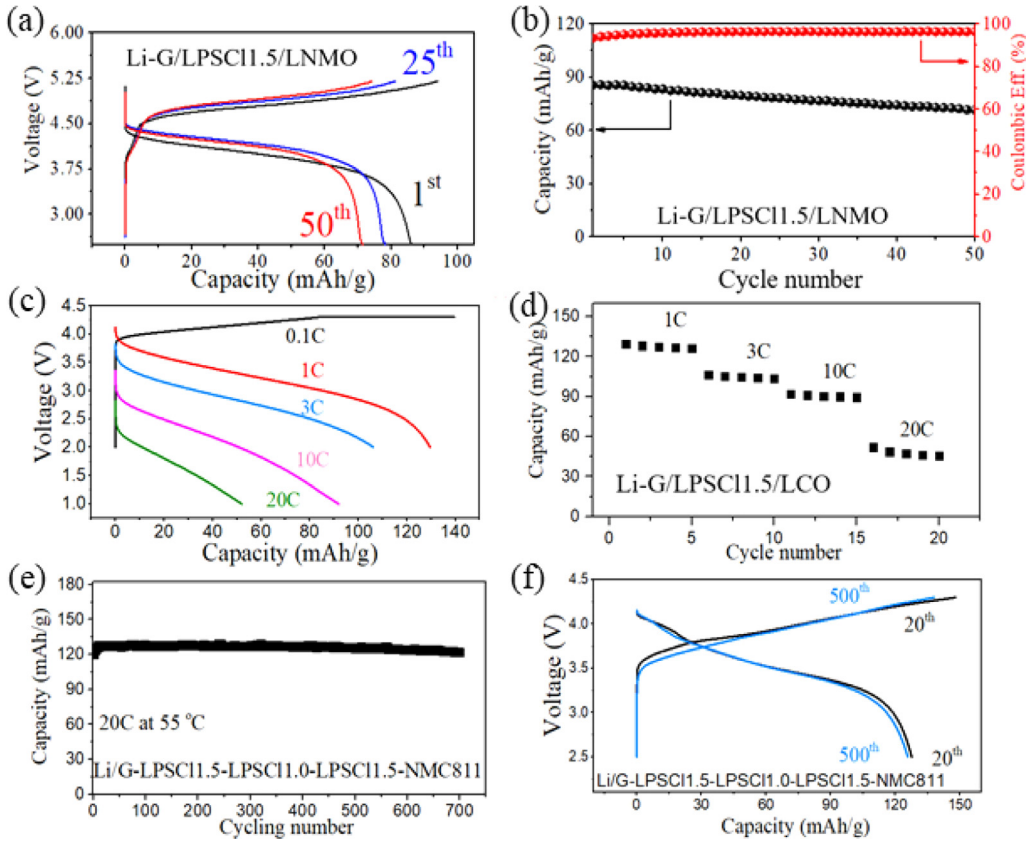

Fig. 3. Galvanostatic charge-discharge voltage profiles and cycling performance of (a,b) Li-G/$Li_{5.5}PS_{4.5}Cl_{1.5}$/LNMO batteries at 0.1C. (c) Voltage profiles and (d) cycling performance of Li-G/ $Li_{5.5}PS_{4.5}Cl_{1.5}$/LCO battery discharged at 1–20 C after charging at 0.1 C and holding voltage at 4.3 V. (e) Voltage profiles and (f) cycling performance of Li-G/ $Li_{5.5}PS_{4.5}Cl_{1.5}$-$Li_6PS_5Cl_1$-$Li_{5.5}PS_{4.5}Cl_{1.5}$/NMC811 batteries at 20 C-rate of continuous charge and discharge. All LCO batteries were cycled at room temperature, LNMO battery and NMC811 battery were cycled at 55 °C.

side to contribute to the decomposition current, significant amount of Li metal can be localized due to sluggish Li^+ transport at the decomposition front under high local stress [27], contributing a significant portion of local positive reaction strains. The localized Li metal, however, will form a layer of decomposition products with the electrolyte that well-enclose itself. Thus, we do not expect the Li metal localized in the cathode region can be easily observed by spectroscopy techniques, while a microscopy technique could be more helpful [49]. However, the significantly widened voltage stability window of LPSCl1.5 by the application of mechanical constriction in our CV tests (Figure S10) is consistent with the voltage window widening from K_{eff} = 0 to K_{eff} = 20 GPa (Fig. 2c, Figure S1e). This supports an assumption underlying our computations, i.e., the localization of Li metal for high positive reaction strains [31]. The localized Li metal is likely stabilized by the surrounding compressive strain field generated by itself, through meta- and kinetic stabilities [27].

All-solid-state batteries were then assembled using Li-graphite layer covered Li metal [30] paired with $LiNi_{0.5}Mn_{1.5}O_4$ (LNMO) and $LiCoO_2$ (LCO). The LNMO cell shows an initial discharge capacity of 85.5 mAh g^{-1} with a high cut-off voltage set at 5.2 V, retaining 84% of the initial discharge capacity at 0.1C after 50 cycles with an average Coulombic efficiency of 98% (Fig. 3a and 3b). The discharge capacities of the LPSCl1.5-LCO cell at 1 C, 3 C, 10 C, and 20 C are 129.6, 106.2, 91.9, and 51.9 mAh/g (Fig. 3c and 3d). The high rate capability is originated from the high ionic conductivity of LPSCl1.5, as well as the stable interphase with cathode materials. However, the pure LPSCl1.5 cell can only be charged at slow rate and cannot sustain a long cycling even with the procedure of slow charge and fast discharge, due to the lithium dendrite penetration at high rates.

In order to prevent the dendrite penetration, a multilayer configuration following our recent approach is constructed [28]. The combination of $Li_{5.5}PS_{4.5}Cl_{1.5}$-$Li_6PS_5Cl_{1.0}$-$Li_{5.5}PS_{4.5}Cl_{1.5}$ or LPSCl1.5-LPSCl1.0-LPSCl1.5, in contrast, advances the high-rate performance and delivers a capacity of 128 mAh/g at 20 C at 55 °C with a 95% capacity retention after 700 cycles (Fig. 3e-3f). The high-rate performance is attributed to the high stability of LPSCl1.5 to both lithium metal and NMC811, as well as the dendrite suppression of the multilayer configuration. The cathode loading is 2 mg/cm^2, where a high current density at up to 20 C applies an electrochemical stress to the solid battery system equivalent to that of a 20 mg/cm^2 loading at 2 C, as they share the same current density. That said, the low loading condition of 2 mg/cm^2 can help us focus more on the understanding of the balance of multiple intrinsic metrics at the electrolyte material level for the ability to suppress the Li dendrite penetration. Higher cathode loading, on the contrary, will complicate the discussion by introducing factors associated with the high thickness of lithium layer in plating. To decouple these factors and simplify the discussion, we focus on the low loading configuration in this paper.

For comparison, batteries with $Li_7P_3S_{11}$ (LPS) and LGPS were also assembled and tested under the same conditions (Figure S11). In every case, the chlorine-rich Li-argyrodites batteries either with LCO or LNMO outperformed those with LPS and LGPS of poorer stability against Li metal and high-voltage cathode materials [50,51]. Previously, we have demonstrated that LGPS has an enhanced high-voltage stability under strong mechanical constriction to be cycled with a 5-V class cathode $LiCo_{0.5}Mn_{1.5}O_2$ with two plateaus at around 4 V and 5 V[27]. LNMO with a long high voltage plateau at 4.7 V, however, applies a higher electrochemical stress to the interface between cathode and electrolyte. Therefore, the fact that LPSCl1.5 can be more stably cycled with LNMO sug-

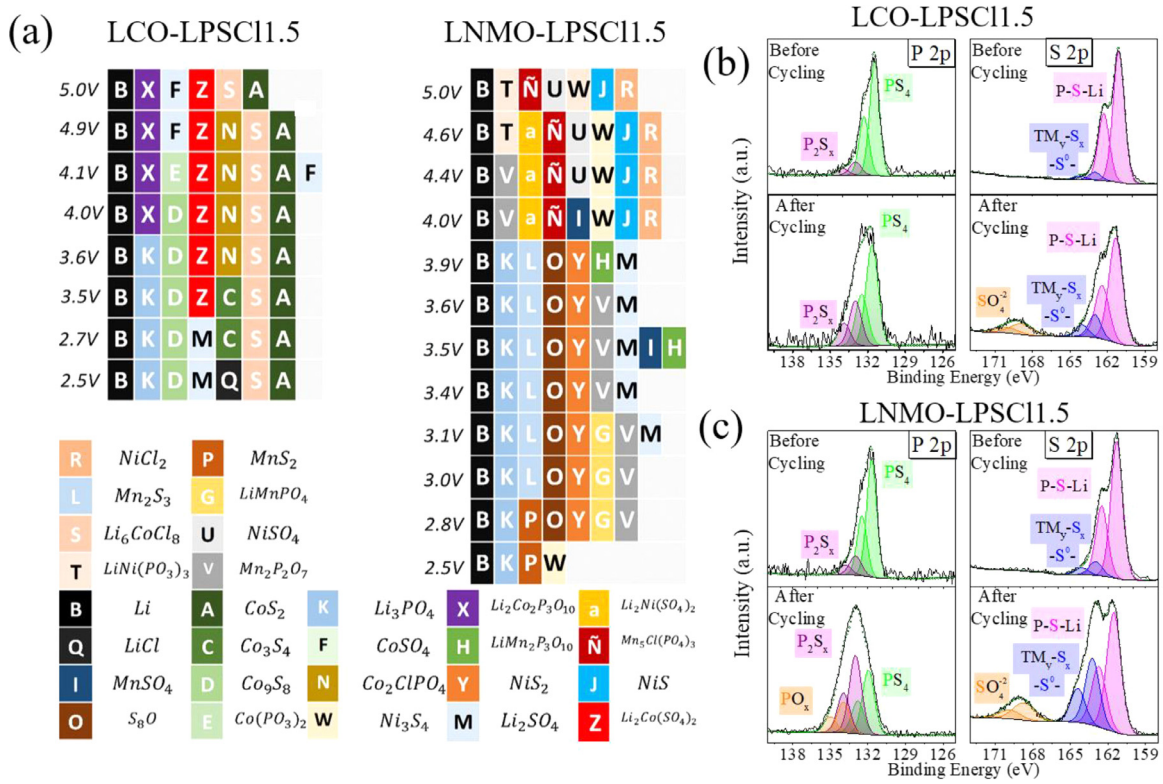

Fig. 4. (a) Predicted LCO-LPSCl1.5 and LNMO-LPSCl1.5 interphase decomposition products in different phase equilibria within each voltage range at K_{eff} = 20 GPa. All decomposition products are the ground state phases within each voltage range. (b) Ex-situ P 2p and S 2p XPS spectra of the LCO electrode of Li/LPSCl1.5/LCO cell before and after cycling. (c) Ex-situ P 2p and S 2p XPS spectra of the LNMO electrode of Li-G/LPSCl1.5/LNMO cell before and after cycling.

gests that the interphase is the most stable at high voltages near 5-V among these three sulfide solid electrolytes.

In order to further understand the degradation mechanism of the cell and the nature of the decomposition products, DFT simulations and ex-situ XPS measurements in the cathode composites after battery cycling were conducted. Note that chemo-mechanical reaction in a complex solid-state battery is dynamic [28,29,31,32] and the local mechanical properties are highly influenced by the interfaces and the associated interface reactions. The pressure applied during battery testing will eliminate voids in the pellets, making it a rigid bulk. Local decomposition tends to happen on the imperfect interfaces and residual voids, as well as the shrinkage of cathode materials such as LNMO upon delithiation [27,52]. In our picture, those imperfections in a dense pellet can be in certain degree compensated by the volume expansion of interface reactions, therefore, a positive interface reaction strain is preferred.

Regarding the nature of decomposition products in the cathode region, Fig. 4a includes the predicted decomposition products for LPSCl1.5-LCO and LPSCl1.5-LNMO interphases at K_{eff} = 20 GPa (corresponding approximately to the mechanical constriction level in real battery testing conditions [29]). The decompositions in experiment were probed by ex-situ XPS measurements carried out in the cathode composites of the LPSCl1.5-LCO and LPSCl1.5-LNMO batteries after cycling. The exact composition of the predicted decomposition products within each voltage range for both LPSCl1.5-LCO and LPSCl1.5-LNMO interphases at K_{eff} = 20 GPa can be found in Table S6. After battery cycling, the LCO cell experienced some oxidation as it can be inferred from the comparison of P 2p and S 2p XPS spectra in Fig. 4b. For instance, the amount of polysulfides and transition metal polysulfides, P_2S_x and TM_y-S_x, increases considerably, as it is observed in both the P 2p and S 2p spectra, which are likely to also include Co_yS_x, among other products, as shown in the prediction of Fig. 4a. In the S2p spectra, sulfates at 169 eV (SO_4^{2-}) are also presented, which could be related to the reaction of the argyrodites with oxygen from the active material [41]. According to the predicted products, these sulfates probably consist of one or more of the lithium sulfates, transition metal sulfates and mixed lithium-transition metal sulfates (Fig. 4a).

Analogous results were obtained from the XPS analysis of the LNMO cell after cycling, as shown in Fig. 4c. However, as expected, the decomposition at the cathode interface is severer than in the LCO-LPSCl1.5 case due to the lower decomposition reaction strain that is harder to be mechanically constricted. Auvergniot et al., who studied the electrochemical stability of L_6PS_5Cl with several cathode materials, including $LiCoO_2$ and the spinel $LiMnO_4$, observed similar decomposition trend [41]. Besides a dramatic increase of polysulfide and transition metal polysulfide species, P_2S_x and TM_y-S_x, including nickel and manganese sulfides, phosphates, PO_x, (probably lithium phosphates, manganese phosphates and mixed lithium-transition metal phosphates as inferred from Fig. 4a) are also presented at 134 eV in the P 2p spectra.

Additionally, these results are in good agreements with those of Figure S12, where the chemical interphase stability of LPSCl1.5 with LCO and LNMO upon heat treatment was evaluated by XRD and XPS [39]. A close examination of the area of the peaks in XPS experiments suggests that the chemical and electrochemical stabilities are similar for these interphases, although a bit more oxidation has been observed chemically than electrochemically for the LPSCl1.5-LNMO interphase. However, X-ray absorption spectroscopy in fluorescence mode (Figure S13), which is bulk-sensitive, does not show obvious oxidation of LPSCl1.5 after high-voltage CV and battery cycling, suggesting that the cathode interphase decompositions are limited at a very thin layer of LPSCl1.5 surface as suggested by the surface-sensitive XPS (Fig. 2b, 4b, 4c). It is worth noting that for NMC811-LPSCl1.5 interface after long cycling (Fig. 3e), similar oxidation of P and S are also observed. The comparison of LCO, LNMO and NMC811 batteries here shows a somewhat decoupling of cycling performance and cathode interphase decomposition when LP-

SCl1.5 is used as the cathode electrolyte, emphasizing the importance of anode stability to Li metal for the cycling of solid state batteries that can be instead enhanced by the multilayer approach.

3. Conclusions

In summary, we show that the synergistic effect of chlorine substitution in sulfide-based SEs along with mechanical constriction leads to a concomitant effect that not only increases the conductivity but also widen the stability window due to higher reaction strain of Cl-related compounds under mechanical constrictions. More importantly, by using Cl content to modulate the balance of low voltage stability and instability of $LPSCl_x$, combined with a multilayer configuration with a hierarchy of electrolyte stabilities to Li metal as a platform for a systematic comparison, we unveil that the functionality of Li dendrite suppression may include the interplay of multiple metrics of decomposition energy, decomposition self-limiting ability, thermodynamic metastability, ionic passivations at low voltages, and possibly structure inhomogeneities that can further tune these metrics. It also shows in the paper that electronic passivation is much less susceptible to chemical compositions than the mechanical constriction effect in governing the different voltage stabilities of sulfide electrolytes based on our circuit model. After cycling with cathode materials, the solid electrolytes in the cathode side shows a similar level of decomposition despite the cyclability, indicating that anode (instead of cathode) stability is probably more responsible for the long-term cyclability in many cases.

The understanding of the chlorine substitution effect along with mechanical constriction in sulfide-based solid electrolytes provides important insights for the chemical design of solid electrolytes and, therefore, the development of all-solid-state batteries.

Declaration of Competing Interest

None.

Acknowledgement

The work was supported by Dean's Competitive Fund for Promising Scholarship at Harvard University, Data Science Initiative Competitive Research Award at Harvard University, and in part by the Global Innovation Contest (GIC) of LG Energy Solution, Ltd. The multilayer configuration related tests (Figure 2e-2l, 3e, 3f, and S8 and S9) are supported by Harvard Climate Change Solutions Fund and Harvard Physical Sciences and Engineering Accelerator Award. E.G.-G. thanks Real Colegio Complutense (RCC) at Harvard for her postdoctoral fellowship. Z. X. is supported by Chinese Scholarship Council (CSC) and the home institution of Shanghai Jiaotong University as a visiting graduate student at Harvard University for one year. Z. S. and E. H. are supported by the Assistant Secretary for Energy Efficiency and Renewable Energy, Vehicle Technology Office of the U.S. DOE through the Advanced Battery Materials Research (BMR) Program, under contract No. DE-SC0012704. This research used beamline 9 BM of the Advanced Photon Source, a U.S. Department of Energy (DOE) Office of Science User Facility operated for the DOE Office of Science by Argonne National Laboratory under contract no. DE-AC02–06CH11357. The XPS and SEM experiments were conducted at the Center for Nanoscale Systems (CNS) at Harvard University, supported by the National Science Foundation.

Author contributions

X.L. conceived the project and supervised all aspects of the research. E.G.-G and L.Y. designed and synthesized the solid electrolyte and performed electrochemical measurements. L.Y. and X. L. designed the multilayer configuration. L. Y. tested the multilayer related batteries (Figure 2e-2l, 3e, and 3f) and conducted the related XPS characterization. E.G.-G. conducted XRD characterization and XPS analysis. Y.W. performed the electrochemical stability related DFT simulations and the decomposition interphase circuit modeling. Z. X. performed the ionic conductivity related Ab-initio molecular dynamics simulations. Z. S. and E. H. performed the XAS characterization. All authors discussed the results. E.G.-G., L.Y., and X.L. analyzed the results and wrote the manuscript.

Supplementary materials

Supplementary material associated with this article can be found, in the online version, at doi:10.1016/j.ensm.2021.12.008.

References

[1] C. Sun, J. Liu, Y. Gong, D.P. Wilkinson, J. Zhang, Recent advances in all-solid-state rechargeable lithium batteries, Nano Energy 33 (2017) 363–386.
[2] K. Takada, Progress and prospective of solid-state lithium batteries, Acta Mater. 61 (2013) 759–770.
[3] A. Manthiram, X. Yu, S. Wang, Lithium battery chemistries enabled by solid-state electrolytes, Nat. Rev. Mater. 2 (2017) 16103.
[4] J.-.M. Tarascon, M. Armand, Issues and challenges facing rechargeable lithium batteries, Nature 414 (2001) 359–367.
[5] H.-.D. Lim, J.-.H. Park, H.-.J. Shin, J. Jeong, J.T. Kim, K.-.W. Nam, H.-.G. Jung, K.Y. Chung, A review of challenges and issues concerning interfaces for all-solid-state batteries, Energy Storage Mater. 25 (2020) 224–250.
[6] Z. Gao, H. Sun, L. Fu, F. Ye, Y. Zhang, W. Luo, Y. Huang, Promises, challenges, and recent progress of inorganic solid-state electrolytes for all-solid-state lithium batteries, Adv. Mater. 30 (2018) 1705702.
[7] Y. He, C. Lu, S. Liu, W. Zheng, J. Luo, Interfacial incompatibility and internal stresses in all-solid-state lithium ion batteries, Adv. Energy Mater. 9 (2019) 1901810.
[8] Y. Kato, S. Hori, T. Saito, K. Suzuki, M. Hirayama, A. Mitsui, M. Yonemura, H. Iba, R. Kanno, High-power all-solid-state batteries using sulfide superionic conductors, Nat. Energy 1 (2016) 16030.
[9] J.B. Goodenough, K.-.S. Park, The Li-ion rechargeable battery: a perspective, J. Am. Chem. Soc. 135 (2013) 1167–1176.
[10] H.-.J. Deiseroth, S.-.T. Kong, H. Eckert, J. Vannahme, C. Reiner, T. Zaiß, M. Schlosser, Li_6PS_5X: a class of crystalline Li-rich solids with an unusually high Li^+ mobility, Angew. Chemie Int. Ed. 47 (2008) 755–758.
[11] S. Wang, Y. Zhang, X. Zhang, T. Liu, Y.-.H. Lin, Y. Shen, L. Li, C.-.W. Nan, High–conductivity argyrodite Li_6PS_5Cl solid electrolytes prepared via optimized sintering processes for all-solid-state lithium-sulfur batteries, ACS Appl. Mater. Interfaces 10 (2018) 42279–42285.
[12] S. Boulineau, M. Courty, J.-.M. Tarascon, V. Viallet, Mechanochemical synthesis of Li-argyrodite Li_6PS_5X (X = Cl, Br, I) as sulfur-based solid electrolytes for all solid state batteries application, Solid State Ionics 221 (2012) 1–5.
[13] C. Yu, S. Ganapathy, J. Hageman, L. van Eijck, E.R.H. van Eck, L. Zhang, T. Schwietert, S. Basak, E.M. Kelder, M. Wagemaker, Facile synthesis toward the optimal structure-conductivity characteristics of the argyrodite Li_6PS_5Cl solid-state electrolyte, ACS Appl. Mater. Interfaces 10 (2018) 33296–33306.
[14] H.-.J. Deiseroth, J. Maier, K. Weichert, V. Nickel, S.-.T. Kong, C. Reiner, Li_7PS_6 and Li_6PS_5X (X: Cl, Br, I): Possible three-dimensional diffusion pathways for lithium ions and temperature dependence of the ionic conductivity by impedance measurements, Zeitschrift für Anorg. und Allg. Chemie 637 (2011) 1287–1294.
[15] S.-.T. Kong, H.-.J. Deiseroth, C. Reiner, Ö. Gün, E. Neumann, C. Ritter, D. Zahn, Lithium argyrodites with phosphorus and arsenic: order and disorder of lithium atoms, crystal chemistry, and phase transitions, Chem. - A Eur. J. 16 (2010) 2198–2206.
[16] N.J.J. de Klerk, I. Rosłoń, M. Wagemaker, Diffusion mechanism of Li argyrodite solid electrolytes for Li-ion batteries and prediction of optimized halogen doping: the effect of Li vacancies, halogens, and halogen disorder, Chem. Mater. 28 (2016) 7955–7963.
[17] C. Yu, Y. Li, M. Willans, Y. Zhao, K.R. Adair, F. Zhao, W. Li, S. Deng, J. Liang, M.N. Banis, R. Li, H. Huang, L. Zhang, R. Yang, S. Lu, Y. Huang, X. Sun, Superionic conductivity in lithium argyrodite solid-state electrolyte by controlled Cl-doping, Nano Energy 69 (2020) 104396.
[18] P. Adeli, J.D. Bazak, K.H. Park, I. Kochetkov, A. Huq, G.R. Goward, L.F. Nazar, Boosting solid-state diffusivity and conductivity in lithium superionic argyrodites by halide substitution, Angew. Chemie Int. Ed. 58 (2019) 8681–8686.
[19] W.D. Jung, J.-.S. Kim, S. Choi, S. Kim, M. Jeon, H.-.G. Jung, K.Y. Chung, J.-.H. Lee, B.-.K. Kim, J.-.H. Lee, H. Kim, Superionic halogen-rich Li-argyrodites using in situ nanocrystal nucleation and rapid crystal growth, Nano Lett. 20 (2020) 2303–2309.
[20] P. Adeli, J.D. Bazak, A. Huq, G.R. Goward, L.F. Nazar, Influence of aliovalent cation substitution and mechanical compression on Li-ion conductivity and diffusivity in argyrodite solid electrolytes, Chem. Mater. 33 (2021) 146–157.
[21] T.K. Schwietert, V.A. Arszelewska, C. Wang, C. Yu, A. Vasileiadis, N.J.J. de Klerk, J. Hageman, T. Hupfer, I. Kerkamm, Y. Xu, E. van der Maas, E.M. Kelder, S. Ganapathy, M. Wagemaker, Clarifying the relationship between redox activity and electrochemical stability in solid electrolytes, Nat. Mater. 19 (2020) 428–435.
[22] Y. Zhu, X. He, Y. Mo, Origin of outstanding stability in the lithium solid electrolyte materials: insights from thermodynamic analyses based on first-principles calculations, ACS Appl. Mater. Interfaces 7 (2015) 23685–23693.
[23] F. Han, Y. Zhu, X. He, Y. Mo, C. Wang, Electrochemical stability of $Li_{10}GeP_2S_{12}$ and $Li_7La_3Zr_2O_{12}$ solid electrolytes, Adv. Energy Mater. 6 (2016) 1–9.

[24] F. Han, T. Gao, Y. Zhu, K.J. Gaskell, C. Wang, A battery made from a single material, Adv. Mater. 27 (2015) 3473–3483.
[25] F. Du, X. Ren, J. Yang, J. Liu, W. Zhang, Structures, thermodynamics, and Li^+ mobility of $Li_{10}GeP_2S_{12}$: a first- principles analysis, J. Phys. Chem. C 118 (20) (2014) 10590–10595.
[26] N. Kamaya, K. Homma, Y. Yamakawa, M. Hirayama, R. Kanno, M. Yonemura, T. Kamiyama, Y. Kato, S. Hama, K. Kawamoto, A lithium superionic conductor, Nat. Mater. 10 (2011) 682–686.
[27] L. Ye, W. Fitzhugh, E. Gil-González, Y. Wang, Y. Su, H. Su, T. Qiao, L. Ma, H. Zhou, E. Hu, X. Li, Toward higher voltage solid-state batteries by metastability and kinetic stability design, Adv. Energy Mater. (2020) 1–13 2001569.
[28] L. Ye, X. Li, A dynamic stability design strategy for lithium metal solid state batteries, Nature 593 (2021) 218–222 DOI:10.1038/s41586-021-03486-3.
[29] W. Fitzhugh, L. Ye, X. Li, The effects of mechanical constriction on the operation of sulfide based solid-state batteries, J. Mater. Chem. A 7 (2019) 23604–23627.
[30] Y. Su, L. Ye, W. Fitzhugh, Y. Wang, E. Gil-González, I. Kim, X. Li, A more stable lithium anode by mechanical constriction for solid state batteries, Energy Environ. Sci. 13 (2020) 908–916.
[31] W. Fitzhugh, F. Wu, L. Ye, H. Su, X. Li, Strain-stabilized ceramic-sulfide electrolytes, Small (2019) 1–14 1901470.
[32] F. Wu, W. Fitzhugh, L. Ye, J. Ning, X. Li, Advanced sulfide solid electrolyte by core-shell structural design, Nat. Commun. 9 (2018) 1–11.
[33] X. Li, Critical assembly and test procedures driven by mechanical constriction principle for advanced performances of solid-state batteries, Adv. Energy Sustain. Res. 2 (2021) 2100003.
[34] R. Prasada Rao, H. Chen, S. Adams, Stable lithium ion conducting thiophosphate solid electrolytes $Li_x(PS_4)_yX_z$ (X = Cl, Br, I), Chem. Mater. (2020) DOI:10.1021/acs.chemmater.9b01926.
[35] T. Asano, A. Sakai, S. Ouchi, M. Sakaida, A. Miyazaki, S. Hasegawa, Solid halide electrolytes with high lithium-ion conductivity for application in 4 V class bulk-type all-solid-state batteries, Adv. Mater. 30 (2018) 1–7.
[36] Z. Zhu, I.-.H. Chu, S.P. Ong, $Li_3Y(PS_4)_2$ and $Li_5PS_4Cl_2$: new lithium superionic conductors predicted from silver thiophosphates using efficiently tiered ab initio molecular dynamics simulations, Chem. Mater. 29 (2017) 2474–2484.
[37] S. Wenzel, D.A. Weber, T. Leichtweiss, M.R. Busche, J. Sann, J. Janek, Interphase formation and degradation of charge transfer kinetics between a lithium metal anode and highly crystalline $Li_7P_3S_{11}$ solid electrolyte, Solid State Ionics 286 (2016) 24–33.
[38] S. Wenzel, S.J. Sedlmaier, C. Dietrich, W.G. Zeier, J. Janek, Interfacial reactivity and interphase growth of argyrodite solid electrolytes at lithium metal electrodes, Solid State Ionics 318 (2018) 102–112.
[39] W. Fitzhugh, F. Wu, L. Ye, W. Deng, P. Qi, X. Li, A high-throughput search for functionally stable interfaces in sulfide solid-state lithium ion conductors, Adv. Energy Mater. 9 (2019) 1–12.
[40] J. Auvergniot, A. Cassel, D. Foix, V. Viallet, V. Seznec, R. Dedryvère, Redox activity of argyrodite Li_6PS_5Cl electrolyte in all-solid-state Li-ion battery: an XPS study, Solid State Ionics 300 (2017) 78–85.
[41] J. Auvergniot, A. Cassel, J.-.B. Ledeuil, V. Viallet, V. Seznec, R. Dedryvère, Interface stability of argyrodite Li_6PS_5Cl toward $LiCoO_2$, $LiNi_{1/3}Co_{1/3}Mn_{1/3}O_2$, and $LiMn_2O_4$ in bulk all-solid-state batteries, Chem. Mater. 29 (2017) 3883–3890.
[42] F. Walther, R. Koerver, T. Fuchs, S. Ohno, J. Sann, M. Rohnke, W.G. Zeier, J. Janek, Visualization of the interfacial decomposition of composite cathodes in argyrodite-based all-solid-state batteries using time-of-flight secondary-ion mass spectrometry, Chem. Mater. 31 (2019) 3745–3755.
[43] F.J. Simon, M. Hanauer, A. Henss, F.H. Richter, J. Janek, Properties of the interphase formed between argyrodite-type Li_6PS_5Cl and polymer-based PEO_{10}:LiTFSI, ACS Appl. Mater. Interfaces 11 (45) (2019) 42186–42196.
[44] W.D. Richards, L.J. Miara, Y. Wang, J.C. Kim, G. Ceder, Interface stability in solid-state batteries, Chem. Mater. 28 (2016) 266–273.
[45] J.M. Doux, H. Nguyen, D.H.S. Tan, A. Banerjee, X. Wang, E.A. Wu, C. Jo, H. Yang, Y.S. Meng, Stack pressure considerations for room-temperature all-solid-state lithium metal batteries, Adv. Energy Mater. 10 (2020) 1–6.
[46] Y.G. Lee, S. Fujiki, C. Jung, N. Suzuki, N. Yashiro, R. Omoda, D.S. Ko, T. Shiratsuchi, T. Sugimoto, S. Ryu, J.H. Ku, T. Watanabe, Y. Park, Y. Aihara, D. Im, I.T. Han, High-energy long-cycling all-solid-state lithium metal batteries enabled by silver-carbon composite anodes, Nat. Energy 5 (2020) 299–308.
[47] Y. Lu, C.Z. Zhao, H. Yuan, X.B. Cheng, J.Q. Huang, Q. Zhang, Critical current density in solid-state lithium metal batteries: mechanism, influences, and strategies, Adv. Funct. Mater. (2020) DOI:10.1002/adfm.202009925.
[48] W. Fitzhugh, X. Chen, Y. Wang, L. Ye, X. Li, Solid-electrolyte-interphase design in constrained ensemble for solid-state batteries, Energy Environ. Sci. 14 (2021) 4574–4583.
[49] X. Liu, R. Garcia-Mendez, A.R. Lupini, Y. Cheng, Z.D. Hood, F. Han, A. Sharafi, J.C. Idrobo, N.J. Dudney, C. Wang, C. Ma, J. Sakamoto and M. Chi, Local electronic structure variation resulting in Li 'filament' formation within solid electrolytes, Nat. Mater., DOI:10.1038/s41563-021-01019-x.
[50] R. Xu, F. Han, X. Ji, X. Fan, J. Tu, C. Wang, Interface engineering of sulfide electrolytes for all-solid-state lithium batteries, Nano Energy 53 (2018) 958–966.
[51] G. Oh, M. Hirayama, O. Kwon, K. Suzuki, R. Kanno, Bulk-type all solid-state batteries with 5V class $LiNi_{0.5}Mn_{1.5}O_4$ cathode and $Li_{10}GeP_2S_{12}$ solid electrolyte, Chem. Mater. 28 (2016) 2634–2640.
[52] K. Ariyoshi, Y. Iwakoshi, N. Nakayama, T. Ohzuku, Topotactic two-phase reactions of $Li[Ni_{1/2}Mn_{3/2}]O_4$ ($P4_332$) in nonaqueous lithium cells, J. Electrochem. Soc. 151 (2004) A296-A303.